

Prescribed nanoparticle cluster architectures and low-dimensional arrays built using octahedral DNA origami frames

*Ye Tian^{1, &}, Tong Wang^{2, &}, Wenyan Liu¹, Huolin L. Xin¹, Huilin Li^{2,3}, Yonggang Ke^{4,5,6#},
William M. Shih^{4,5,6}, and Oleg Gang^{1*}*

¹Center for Functional Nanomaterials, Brookhaven National Laboratory, Upton, NY 11973, USA

²Biosciences Department, Brookhaven National Laboratory, Upton, NY 11973, USA

³Department of Biochemistry and Cell Biology, Stony Brook University, Stony Brook, NY 11794-5213, USA

⁴Department of Biological Chemistry and Molecular Pharmacology, Harvard Medical School, Boston, MA, 02115, USA

⁵Department of Cancer Biology, Dana-Farber Cancer Institute, Boston, MA, 02115, USA

⁶Wyss Institute for Biologically Inspired Engineering, Harvard University, Boston, MA, 02115, USA

[&]These authors contributed equally to this work

[#]Present Address: Department of Biomedical Engineering, Georgia Institute of Technology and Emory University, Atlanta, GA 30322, USA

^{*}*ogang@bnl.gov*

Three-dimensional mesoscale clusters that are formed from nanoparticles spatially arranged in pre-determined positions can be thought of as mesoscale analogues of molecules. These nanoparticle architectures could offer tailored properties due to collective effects, but developing a general platform for fabricating such clusters is a significant challenge. Here, we report a strategy for assembling 3D nanoparticle clusters that uses a molecular frame designed with encoded vertices for particle placement. The frame is a DNA origami octahedron and can be used to fabricate clusters with various symmetries and particle compositions. Cryo-electron microscopy is used to uncover the structure of the DNA frame and to reveal that the nanoparticles are spatially coordinated in the prescribed manner. We show that the DNA frame and one set of nanoparticles can be used to create nanoclusters with different chiroptical activities. We also show that the octahedra can serve as programmable interparticle linkers, allowing one- and two-dimensional arrays to be assembled that have designed particle arrangements.

The assembly of well-defined particle clusters by design has long been seen as one of the key challenges in rational material fabrication due to their direct analogy with molecules. The designed clusters are not constrained by the orientations of interatomic bonds as in molecules found in the natural world. Therefore, a broad diversity of structures can potentially be generated. Clusters with tailored structures and functions could be used as the designer's blocks to create higher level organizations. Such clusters were recently proposed for addressing the challenge of inverse engineering in self-assembled systems^{1,2}. From a functional perspective, designed meso-clusters from nanoparticles are attractive for accessing their collective and synergetic effects³⁻⁶ and manipulating their optical response^{3,7-9}.

Recently, much progress was achieved on micron-scales in understanding and fabrication of clusters from so called patchy particles¹⁰, where the placement of patches determines directional interparticle interactions^{11,12}. For nanoscale particles, the challenges in placing patterns in the specified particle's locations with a high fidelity are significant; therefore, alternative strategies were considered. A number of studies explored the DNA-assembled hetero-clusters¹³, the discrete and polymer-like¹⁴ assemblies using nanoparticles with monovalent and multivalent binding properties^{4,13-16}, step-wise assembly from molecularly encoded surfaces¹⁷, and via templating of molecular motifs¹⁸⁻²⁰. Nevertheless, methods for robust and massive assembly of complex yet designed cluster architectures in which nanoparticles of different types can be spatially arranged in pre-determined three-dimensional (3D) arrangements remain challenging. Furthermore, an ultimate goal is a development of universal assembly platform that can be applied to a wide range of nanoparticles materials and their surface functionalities.

In this paper we propose and demonstrate the experimental realization of the nanoparticle cluster assembly platform using a rigid 3D nanoscale molecular frame. We show in the specific implementation using an octahedral DNA frame that nanoparticles can be arranged in 3D in the prescribed locations, which are determined by the frame vertices encoded by the specific DNA sequences (Figure 1). We show several representative examples of particles organizations: (i) an octahedral cluster that fully

replicates the frame geometry (Figure 1b); (ii) a square-like cluster in which subset symmetry of the original frame is used (Figure 1c); (iii) an octahedral hetero-cluster in which three types of particles are coordinated in the particular positions (Figure 1d). We stress that the discussed approach is conceptually different from the assembly methods based on patchy and patterned particles, since no complex particle fabrication is required. As we show below, the proposed methodology, “the cluster assembly by frame”, streamlines a fabrication of designed 3D meso-architectures and fully support the integration of different nanoparticle types as soon as they contain specific DNAs in their shell ^{21,22}. We choose to use DNA as a frame for the implementation of the concept due to its highly customizable structure ²³ and ease of programmability of interactions between the frame and particles. Over the past decade, DNA have offered a compelling methods towards creation of nanoparticles arrays, either in 2D using DNA tile motifs ^{24,25} by implementing basic design rules ²³ or in 3D using DNA-encoded particle shell interactions ^{26,27}, as well as discrete assemblies and linear arrays ^{4,8,18}. The DNA origami technology allows for the designed fabrication of discrete 2D ²⁸ and 3D ²⁹ DNA shapes, and the reactive groups can be precisely located ³⁰. We use here 3D origami construct, shaped as octahedron with DNA-encoded vertices, as frame for assembly of designed clusters from nanoparticles. Moreover, we show that their optical response, a chiroptical activity ^{4,7,8}, can be fully controlled based on the prescribed placement of nanoparticles of different sizes on the same central-symmetrical frame. By exploiting the octahedron frame as a programmable linker between nanoparticles we demonstrate, using ex-situ TEM and in-situ x-ray scattering methods, that low-dimensional, linear 1D and square 2D, nanoparticle arrays can be successfully created in the designed manner.

Revealing 3D structure of mesoscale clusters is a significant challenge, particularly, due to the need for probing clusters both on ensemble and individual cluster levels at different scales. Such probing of frame internal structure, 3D positioning of nanoparticles and a cluster population analysis are important for the realization of high-fidelity assembly and understanding the effects of frame-nanoparticle interactions. Traditional TEM provides clear images of metal nanoparticles alone ³¹, but not of the DNA constructs. Negative staining EM offers a way of observing both metal particles and DNA template ^{8,18,30}, but can flatten thus distort the relatively large 3D structure. In

contrast, cryo-electron microscopy (cryo-EM) preserves samples in their near native states and provides close to nanometre resolution of structures using single particle 3D reconstruction technique^{24,32-34} and tomography³⁵⁻³⁷. We show here that cryo-EM can be successfully applied to probe the 3D structure of DNA-nanoparticle clusters.

Structure of octahedral frame and prescribed nanoclusters

First, we designed the frame, an octahedral DNA origami structure (Figure 1a)³⁸ with each edge containing a six-helix-bundle (6HB)³⁹⁻⁴¹. Vertex positions (labelled from 1 to 6) could be encoded with distinctive ssDNA “sticky ends”, which can bind the nanoparticles coated with complementary DNA. We designed three routes to assemble different numbers and sizes of gold nanoparticles (Figure 1b-1d). When six vertices have the same sticky end, a six-particle cluster is formed after mixing with the corresponding DNA-encoded nanoparticles. The resulting nanoparticle cluster, denoted as ‘P₆’ (Figure 1b), has a symmetry O_h. When only four in-plane vertices are encoded and two others are silent, 4-particle cluster (Figure 1c) could be formed, denoted as ‘P₄(1234)’ to indicate the number of particles and their vertex locations. The heterogeneous cluster can be created by introduction of different DNA at vertices of choice. Here, we used three distinctive sets of sticky ends, with two of the same kind located at opposite vertices, as shown in Figure 1d. Such design allows binding three types of nanoparticles. We used 7 nm (P¹), 10 nm (P²), and 15 nm (P³) gold nanoparticle (see supplementary information) with respectively complementary shells for prescribing this hetero-cluster, labelled as ‘P¹₂(12)P²₂(34)P³₂(56)’. The high-fidelity octahedral formation (TEM observed yield around 99%) is clearly visible in the raw cryo-EM micrograph (Figure 2a). The DNA octahedra are randomly oriented in the vitreous ice, have expected dimensions, and appear monodisperse in shape and size. These 2D images permitted computational reconstruction of the 3D structure of the octahedron origami (see supplementary information), as we discuss below. 2D class averages of raw particle images are nearly identical to the corresponding re-projections of the reconstructed 3D density model (Figure 2b). This demonstrates the quality of the particle images and the reliability of the 3D reconstruction of the DNA octahedron.

The 3D density map is surface rendered and shown in the typical 4-fold, 3-fold, 2-fold axis views (Figure 2c). The octahedral edge in the three-dimensional map is ~29 nm long, in agreement with the designed length of 28.6nm. Each edge of the reconstructed DNA octahedron is a hollow structure with a ~2 nm channel in the middle. Again this feature is consistent with our six-helix bundle design for the edge (Figures 1 and Supplementary Figure 3). We therefore chose the six-helix bundle (6HB) design to construct octahedron edges. The hollow structure of 6HB and formed octahedral vertices provides housing functionalized moieties, with potential applications in nanotechnology and biomedicine³⁰. Our success in visualizing the structure of the large, symmetric, and non-space-filling 3D origami constructs by cryo-EM is notable, because this method was previously applied only to the space-filling DNA origami³⁴ or flexible origami box³² or to the nano-scale non-origami polyhedra^{24,32,33}.

We then assembled a simple P_6 cluster on the octahedron frame using 30-base ssDNA functionalized 7-nm gold nanoparticles. We show in Figure 3a a representative raw image of the purified complexes. These clusters are highly homogeneous, with over 90% out of the 460 clusters counted containing the correct number (6) of nanoparticles in the prescribed vertex positions in each octahedron (Figure 3a inset).

It is clear that the 6 nanoparticles of the individual clusters in the raw cryo-EM images are arranged in a manner that is consistent with the octahedral symmetry (Figure 3b). Notably, the DNA is barely visible, with much weaker contrast than the gold nanoparticles. This is because the gold nanoparticles are significantly more electron dense than the DNA. So we calculated two independent 3D reconstructions from the same cryo-EM dataset: in the first reconstruction, the high nanoparticle densities were computationally removed from the raw images, keeping the DNA density intact (Supplementary Figure 5b), and in the second reconstruction the lower intensity DNA density as well as the background noise were removed leaving only the higher intensity nanoparticles (Supplementary Figure 5c). We normalized and then aligned the two reconstructions by their symmetry axes and merged them into a synthetic structure (Figure 3c). In this compound map, the diameters of nanoparticles are around 7 nm, consistent with the particle size estimated from the raw images. Six nanoparticles are

precisely positioned at the six vertices of the reconstructed DNA octahedron frame, with the nearest centre-to-centre interparticle distance of ~ 42 nm.

The control over the assembly of pre-defined cluster, $P_4(1234)$, with a square-like particle arrangement, was further demonstrated by choosing four co-planar corners of the octahedron with the specific sticky end oligonucleotides (Figure 1c). Accordingly, 10 nm nanoparticles with complementary ssDNA shell were assembled in such P_4 cluster. The population histogram (Figure 3d) demonstrates that about 80% of the clusters contains the correct number (four) of nanoparticles (out of total number 554). Figure 3e compares cryo-EM images of six representative origami-nanoparticle clusters with their corresponding views of the 3D model. To illustrate the arrangement of the four nanoparticles on the DNA octahedra, we computed a composite map (Figure 3f) by aligning and merging the gold nanoparticles reconstruction with the DNA octahedron reconstruction, shown in the Figure 2c. The nanoparticle size in the reconstruction is about 10 nm, which is consistent with the estimation from the raw images, and the nearest centre-to-centre interparticle distance is about 40 nm. Thus, four nanoparticles are precisely positioned at the pre-defined octahedron vertices forming the prescribed P_4 cluster.

Next we demonstrate that outlined assembly approach allows for the realization of hetero-clusters containing several types of particles in pre-defined positions. For example, the cluster was designed to coordinate three particles types, $P^1_2(12)P^2_2(34)P^3_2(56)$, as shown in Figure 1d. Six corners of the octahedron were grouped into three diagonal sets. By providing the corresponding DNA encoding, we assign vertices 1 and 2, 3 and 4, and 5 and 6 to bind to 7nm, 10 nm and 15 nm nanoparticles respectively. The representative TEM image of the assembled cluster shows that the majority of these clusters have the correct structure (Supplementary Figure 8). The population histogram (Figure 4a) reveals that about 70% of the clusters (out of a total number of 467 clusters), coordinate 6 nanoparticles with about equal fraction of each particle type. For partially assembled clusters (5 nanoparticles and less), the missing nanoparticles came from 3 different kinds nearly evenly. We note that due to the high dynamical range of electron densities the DNA is nearly invisible.

To unravel the 3D coordinates of the assembled $P^1_2P^2_2P^3_2$ cluster, we apply tomographic method for this system that permit a 3D probing of individual clusters. The TEM image inserted in Figure 4a shows the untilted picture of the cluster which corresponds to reconstructed particles positions (Figure 4b), while Figure 4c presents a few selected tilted images of the reconstruction at -20° , -10° , 20° , 40° , 60° tilt angles. The projections of the reconstructed clusters agreed well with the raw EM images. The averaged surface-to-surface distances, d_7 , d_{10} and d_{15} , between nanoparticles of the same sizes, 7 nm, 10 nm and 15 nm respectively were obtained from twelve reconstructed clusters (Figure 4d). Small but progressive decrease of interparticle distances by about 4 nm is observed when nanoparticle diameter decreases from 15 nm to 7 nm. This change may result from different curvature of particles due to the dependence of DNA length in a shell on particle size⁴². Also, due to a larger attachment area of vertex's DNA for bigger particles, a strain might be imposed on the octahedron resulting in its distortion. Averaged basal (α) and vertex (β , for 15 nm nanoparticle) angles, as noted in Figure 4b, exhibit the well-defined positions of all nanoparticles attached to octahedral frame, as shown in Figure 4e. Ideal basal angle is around 90° which matches our experimental data; while the vertex angle ($54.5^\circ \pm 10.0^\circ$) is close to the expected value of $\sim 56^\circ$. Thus, we conclude that even attachment of larger particles (15 nm Au core) introduce practically no distortion on the frame; this further support the potential use of the approach for assembly of various designer hetero-cluster.

Chiroptical activity of hetero-clusters

The ability to assemble nanoparticle clusters in the designed manner opens new opportunities for creating materials with regulated functions. For example, the chiroptical activity might be induced for plasmonically coupled spherical nanoparticles placed on the chiral⁸ or tetrahedral scaffold⁴. However, as we show here, even the center-symmetric frame, like octahedron, allows producing a chiroptical response if particles of different sizes are placed accordingly. In this case, the chirality is determined by the position of specifically encoded vertices that, in turn, prescribe the placement of different particles. More specifically, depending on the arrangement of nanoparticles of three sizes on the vertices of octahedron, either in the symmetric fashion, similar to $P^1_2P^2_2P^3_2$ (Figure 4) or

in the non-symmetric way, non-chiral or chiral architectures can be formed (Figure 5a and b). Thus, from the same set of particles and the same, but differently encoded, octahedron frame different chiroptical signatures can be generated.

To realize this idea experimentally, we have substituted the 5 nm P_1 particle in $P^1_2P^2_2P^3_2$ with 20nm gold nanoparticle (P_4) in order to increase the cluster plasmonic response. Such new cluster $P^2_2(36)P^3_2(25)P^4_2(14)$, denoted as $P^2_2P^3_2P^4_2$ (Figure 5a), has the same-size particles placed symmetrically (see also the cluster top view in Figure 5a). Representative TEM image of the $P^2_2P^3_2P^4_2$ cluster with the correspondingly oriented model are shown on the top right inset of Figure 5c. No circular dichroism (CD) signal was detected in the plasmonic region of the spectrum (Figure 5c, red line) for such cluster. However, when the 3 pairs of nanoparticles are positioned in the asymmetric arrangement (Figure 5b), the resulting octahedral cluster has left-handed chirality⁴³, as can be verified by the counter-clockwise rotation of 1-3-5 positions of distinguished particles to match the 4-6-2 positions of their twins. Indeed, the cluster, $P^2_2(26)P^3_2(35)P^4_2(14)$, denoted as $P^2_{c2}P^3_{c2}P^4_{c2}$, contains three nanoparticle pairs with the same kinds of nanoparticles placed at the edge ends. Representative TEM image and the corresponding model are shown at the bottom left inset of Figure 5c. For this $P^2_{c2}P^3_{c2}P^4_{c2}$ cluster a negative CD signal was observed (Figure 5c, black line), with its centre at the plasmonic peak of the gold cluster (the absorption curves are shown on Supplementary Figure 12), corresponding to the cluster's left-handed structural chirality. We note that only a very small difference, <1 nm, between plasmonic peak positions for both cases was observed, while, the dramatically different chiroptical responses are exhibited for the symmetric and asymmetric clusters. Interestingly, even the weak plasmonic coupling between nanoparticles (Supplementary Figure 12) in our system due to relatively large separations (about 36 nm surface-to-surface distances) can be still translated into the observable CD response. Thus, we demonstrated that the same set of nanoparticles and the same centre-symmetric frame could be used to produce clusters with optically different CD responses via a simple, but precise, spatial placements of nanoparticles in the 3D cluster.

Designed 1D and 2D nanoparticle arrays

We have further explored the use of the specifically encoded octahedron frame as linking element between nanoparticles for building low-dimensional, 1D and 2D, nanoparticle arrays. In this case the linking symmetry and the resulting structure of the array are determined by the choice of octahedron vertices utilized for inter-particle connections. Unlike assembly approaches utilizing particle positioning on DNA-scaffolds, in the presented strategy, nanoparticles and DNAs are integrated in the unified structure, in which the topology of interparticle connections is fully prescribed by the encoding of octahedra vertices. We prescribe these 1D and 2D arrays by encoding the octahedron to carry 2-fold (Figure 6a) and 4-fold (Figure 6d) symmetries, respectively. More specifically, the frame with 2-fold symmetry contains two vertices with encoding for particle recognition at two ends of the major octahedron diagonal; consequently, this design should result in the linear arrangements of nanoparticles linked by the 2-fold linking frame. Expanding this approach, we can direct the assembly of a 2D square array (D4 symmetry) by encoding the four octahedron vertices, lying in the same plane, for nanoparticles binding. Details for obtaining low dimensional array were described in method section. The samples were then loaded into a glass capillaries and probed by Small Angle X-ray Scattering (SAXS), as previously described^{21,26}.

The structure factor for the nanoparticle assembly induced by the two-fold encoded octahedron (Figure 6c) exhibits five peaks, with peak position located at $q/q_1 \sim 1, 1.8, 2.7, 3.5, 4.3$ (q_1 is the position of the first peak). Such structure factor can be reasonably well described (Figure 6c, blue curve) by dumbbell model^{44,45} with functional form $S(q) \sim \sin(dq)/dq$, where d is a distance between the nanoparticle centres, thus, indicating scattering signature of the nanoparticle pairs. The flexibility of 1D array at the points of octahedron attachment to nanoparticles and the large angle over which the attachment can occur, contribute to the non-collinearity of 1D array. The fit yields $d=67.4$ nm, which is close to, the expected value based on the design parameters. We further confirmed (Figure 6b) the structure of this array by TEM imaging, which shows the morphology and inter-nanoparticle distance ($d=63$ nm), in agreement with the in-situ SAXS results.

The structure of assembly induced by the octahedron with 4-fold symmetry nanoparticle connection was initially revealed by SAXS. The observed $S(q)$ peaks signify a 2D nanoparticle square array (Figure 6f) with interparticle distance of 47.5nm, which is in agreement with 46.4nm obtained from the model (see supplementary information). The deviation of higher order peaks towards larger q from the calculated values can be attributed to the flexibility of 2D nanoparticle-octahedron sheet in the solution. Such structure agrees with the array design (Figure 6e, left model). Indeed, in the formed 2D square arrays the four in-plane vertices (Figure 6d) are bound to four gold nanoparticles, while each nanoparticle binds four octahedra (the vertices below and above the plane are silent). The size of 2D crystallites is 0.2 μm , as estimated from the scattering peak width, and their melting temperature is about 39 $^{\circ}\text{C}$, as detected by DLS measurements (Supplementary Figure 14). The ex-situ visualization with TEM (Figure 6e, right) concurs with the SAXS results, and it closely resembles the model arrangement: a 2D square array of nanoparticles in which they are linked by 4-fold binding octahedron.

Conclusion

The presented studies demonstrate that three-dimensional nanoparticle clusters can be effectively created using the strategy based on the rigid 3D DNA frame with encoded sites for nanoparticles positioning. The example of such approach based on the octahedron, allows for arranging particles in 3D with nearly nanometre precision in the designed non-periodic structure, as confirmed by our detailed visualization using cryo-EM methods. Based on such precise cluster assembly, nano-architectures with different chiroptical activities were created using the same set of nanoparticles but different frame encodings. Moreover, we demonstrated that the designed arrangement of nanoparticles in 1D and 2D arrays could be achieved by prescribing specific vertices of octahedron as nanoparticle connecting sites. The structural integrity of DNA frame ensures proper nanoparticles coordination, while DNA origami methodology provides a predictable frame fabrication. Our work opens up numerous exciting opportunities for high-yield precise assembly of tailored 3D mesoscale building blocks, in which multiple nanoparticles of different structures and functions can be integrated.

References

- 1 Halverson, J.D. & Tkachenko, A.V. DNA-programmed mesoscopic architecture. *Phys. Rev. E* **87**, 062310 (2013).
- 2 Zeravcic, Z. & Brenner, M.P. Self-replicating colloidal clusters. *Proc. Natl Acad. Sci. USA* **111**, 1748-1753 (2013).
- 3 Maye, M.M., Gang, O. & Cotlet, M. Photoluminescence enhancement in CdSe/ZnS-DNA linked-Au nanoparticle heterodimers probed by single molecule spectroscopy. *Chem. Commun.* **46**, 6111-6113 (2010).
- 4 Yan, W. *et al.* Self-assembly of chiral nanoparticle pyramids with strong R/S optical Activity. *J. Am. Chem. Soc.* **134**, 15114–15121 (2012).
- 5 Fan, J.A. *et al.* plasmonic mode engineering with templated self-assembled nanoclusters. *Nano Lett.* **12**, 5318-5324 (2012).
- 6 Hiroi, K., Komatsu, K. & Sato, T. Superspin glass originating from dipolar interaction with controlled interparticle distance among gamma-Fe₂O₃ nanoparticles with silica shells. *Phys. Rev. B* **83**, 224423 (2011).
- 7 Govorov, A.O., Fan, Z., Hernandez, P., Slocik, J.M. & Naik, R.R. Theory of circular dichroism of nanomaterials comprising chiral molecules and nanocrystals: plasmon enhancement, dipole interactions, and dielectric effects. *Nano Lett.* **10**, 1374-1382 (2010).
- 8 Kuzyk, A. *et al.* DNA-based self-assembly of chiral plasmonic nanostructures with tailored optical response. *Nature* **483**, 311-314 (2012).
- 9 Barrow, S.J., Wei, X., Baldauf, J.S., Funston, A.M. & Mulvaney, P. The surface plasmon modes of self-assembled gold nanocrystals. *Nat. Commun.* **3**, 1-9 (2012).
- 10 Ruzicka, B. *et al.* Observation of empty liquids and equilibrium gels in a colloidal clay. *Nature Mater.* **10**, 56-60 (2011).
- 11 Wang, Y. *et al.* Colloids with valence and specific directional bonding. *Nature* **491**, 51-56 (2012).
- 12 Chen, Q. *et al.* Supracolloidal reaction kinetics of janus spheres. *Science* **331**, 199-202 (2011).
- 13 Mastroianni, A.J., Claridge, S.A. & Alivisatos, A.P. Pyramidal and chiral groupings of gold nanocrystals assembled using DNA scaffolds. *J. Am. Chem. Soc.* **131**, 8455–8459 (2009).
- 14 Klinkova, A., Thérien-Aubin, H., Choueiri, R.M., Rubinstein, M. & Kumacheva, E. Colloidal analogs of molecular chain stoppers. *Proc. Natl Acad. Sci. USA* **110**, 18775-18779 (2013).
- 15 Kim, J.-W., Kim, J.-H. & Deaton, R. DNA-linked nanoparticle building blocks for programmable matter. *Angew. Chem. Int. Ed.* **50**, 9185 –9190 (2011).
- 16 Alivisatos, A.P. *et al.* Organization of 'nanocrystal molecules' using DNA. *Nature* **382**, 609-611 (1996).
- 17 Maye, M.M., Nykypanchuk, D., Cuisinier, M., van der Lelie, D. & Gang, O. Stepwise surface encoding for high-throughput assembly of nanoclusters. *Nature Mater.* **8**, 388-391 (2009).
- 18 Pal, S., Deng, Z., Ding, B., Yan, H. & Liu, Y. DNA-origami-directed self-assembly of discrete silver-nanoparticle architectures. *Angew. Chem. Int. Ed.* **49**, 2700–2704 (2010).

- 19 Lee, J., Hernandez, P., Govorov, A.O. & Kotov, N.A. Exciton–plasmon interactions in molecular spring assemblies of nanowires and wavelength-based protein detection. *Nature Mater.* **6**, 291-295 (2007).
- 20 Sun, D. *et al.* Heterogeneous nanoclusters assembled by PNA-templated double-stranded DNA. *Nanoscale* **4**, 6722-6725 (2012).
- 21 Zhang, Y., Lu, F., Yager, K.G., van der Lelie, D. & Gang, O. A general strategy for the DNA-mediated self-assembly of functional nanoparticles into heterogeneous systems. *Nature Nanotech.* **8**, 865-872 (2013).
- 22 Zhang, C. *et al.* A general approach to DNA-programmable atom equivalents. *Nature Mater.* **12**, 741-746 (2013).
- 23 Seeman, N.C. DNA in a material world. *Nature* **421**, 427-431 (2003).
- 24 Shih, W.M., Quispe, J.D. & Joyce, G.F. A 1.7-kilobase single-stranded DNA that folds into a nanoscale octahedron. *Nature* **427**, 618-621 (2004).
- 25 Zheng, J. *et al.* From molecular to macroscopic via the rational design of a self-assembled 3D DNA crystal. *Nature* **461**, 74-77 (2009).
- 26 Nykypanchuk, D., Maye, M.M., van der Lelie, D. & Gang, O. DNA-guided crystallization of colloidal nanoparticles. *Nature* **451**, 549-552 (2008).
- 27 Park, S.Y. *et al.* DNA-programmable nanoparticle crystallization. *Nature* **451**, 553-556 (2008).
- 28 Rothemund, P.W.K. Folding DNA to create nanoscale shapes and patterns. *Nature* **440**, 297-302 (2006).
- 29 Dietz, H., Douglas, S.M. & Shih, W.M. Folding DNA into twisted and curved nanoscale shapes. *Science* **325**, 725-730 (2009).
- 30 Zhang, C. *et al.* DNA nanocages swallow gold nanoparticles (AuNPs) to form AuNP@DNA cage core-shell structures. *ACS Nano* **8**, 1130-1135 (2014).
- 31 Sharma, J. *et al.* Control of self-assembly of DNA tubules through integration of gold nanoparticles. *Science* **323**, 112-116 (2009).
- 32 Andersen, E.S. *et al.* Self-assembly of a nanoscale DNA box with a controllable lid. *Nature* **459**, 73-76 (2009).
- 33 He, Y. *et al.* Hierarchical self-assembly of DNA into symmetric supramolecular polyhedra. *Nature* **452**, 198-201 (2008).
- 34 Bai, X., Martin, T.G., Scheres, S.H.W. & Dietz, H. Cryo-EM structure of a 3D DNA-origami object. *Proc. Natl Acad. Sci. USA* **149**, 20012-20017 (2012).
- 35 Midgley, P.A. & Dunin-borkowski, R.e. electron tomography and holography in materials science. *Nature Mater.* **8**, 271-280 (2009).
- 36 Kourkoutis, L.F., Plitzko, J.M. & Baumeister, W. Electron microscopy of biological materials at the nanometer scale. *Annu. Rev. Mater. Res.* **42**, 33-58 (2012).
- 37 De-Rosier, D. & Klug, A. Reconstruction of three dimensional structures from electron micrographs. *Nature* **217**, 130-134 (1968).
- 38 Douglas, S.M. *et al.* Rapid prototyping of 3D DNA-origami shapes with caDNAno. *Nucleic Acids Res.* **37**, 5001-5006 (2009).
- 39 Mathieu, F. *et al.* Six-helix bundles designed from DNA. *Nano Lett.* **5**, 661-665 (2005).
- 40 Douglas, S.M. *et al.* Self-assembly of DNA into nanoscale three-dimensional shapes. *Nature* **459**, 414-418 (2009).

- 41 Douglas, S.M., Chou, J.J. & Shih, W.M. DNA-nanotube-induced alignment of membrane proteins for NMR structure determination. *Proc. Natl Acad. Sci. USA* **104**, 6644-6648 (2006).
- 42 Hill, H.D., Millstone, J.E., Banholzer, M.J. & Mirkin, C.A. The role radius of curvature plays in thiolated oligonucleotide loading on gold nanoparticles. *ACS Nano* **3**, 418-424 (2009).
- 43 King, R.B. Nonhanded chirality in octahedral metal complexes. *Chirality* **13**, 465-473 (2001).
- 44 Chi, C., Vargas-Lara, F., Tkachenko, A.V., Starr, F.W. & Gang, O. Internal structure of nanoparticle dimers linked by DNA. *ACS Nano* **6**, 6793-7802 (2012).
- 45 Kaya, H. Scattering from cylinders with globular end-caps. *J. Appl. Crystallogr.* **37**, 223-230 (2004).

Acknowledgements

The authors thank J. Li for help with tomography analysis and D. Chen for assistance with schematic drawing. Research carried out at the Centre for Functional Nanomaterials, Brookhaven National Laboratory was supported by the U.S. Department of Energy, Office of Basic Energy Sciences, under Contract No. DE-SC0012704. H.L. was supported by NIH R01 grant AG029979, and W.M.S. was supported by NSF Expeditions grant 1317694 and NSF DMREF grant 1435964.

Author contributions

Y.T. and O.G. conceived and designed the experiments. Y.T. performed the experiments. W.M.S and Y.K. contributed to the octahedral design. Y.T., T.W., W.L. and O.G. analysed the data. T.W. and H.L. contributed to the cryo-EM measurement and reconstruction. H.X. contributed to the tomography analysis. Y.T. and O.G. wrote the paper. O.G. supervised the project. All authors discussed the results and commented on the manuscript.

Additional information

Supplementary information accompanies this paper at www.nature.com/naturenanotechnology. Reprints and permission information is available online at <http://npg.nature.com/reprintsandpermissions/>. Correspondence and requests for materials should be addressed to O.G.

Competing financial interests

The authors declare no competing financial interests.

Figure 1. Scheme of three designed clusters assembled from DNA functionalized gold nanoparticles on correspondingly encoded vertices of DNA octahedral frames.

a, The designed octahedral origami structure. Red numbers mark the six corners or vertices of the octahedron. One vertex is zoomed in the lower panel to show the end-on view of the designed structure comprised of four six-helix bundles (6HB). Each 6HB contains one ssDNA sticky end (dotted blue line) that provides encoding. **b**, An octahedron with all sticky ends being encoded to coordinate 7-nm nanoparticles into the symmetric 6-nanoparticle cluster P_6 . **c**, The $P_4(1234)$ cluster structure may form if the ssDNA at vertices 1-2-3-4 of the octahedral frame is programmed with sequence complementary to the ssDNA on the 10-nm gold nanoparticles. **d**, The $P_1^2(12)P_2^2(34)P_3^2(56)$ cluster structure may assemble if the ssDNA at vertices 1-2, 3-4, and 5-6 are programmed to complement the ssDNA on the 7-nm, 15-nm, and the 10-nm nanoparticles, respectively.

Figure 2. The structure of the self-assembled DNA origami octahedron obtained by Cryo-EM and 3D reconstruction.

a, A cryo-EM micrograph with representative views of DNA octahedron boxed by a black square. Only cluster structures that were embedded in the vitreous ice and suspended over the irregular holes in the carbon film substrate were selected for further analysis. **b**, Comparison of 2D re-projections of the reconstructed 3D density map (top row), with reference-based class averages (second row), reference-free class averages (third row), and with the corresponding views of the 3D design model (bottom row). **c**, Surface-rendered 3D density map of the DNA octahedron, as viewed from the 4-fold (left), 3-fold (middle), and 2-fold (right) symmetry axis. The density surface is coloured radially from interior red to outer blue. The colour key is shown on the right. The values in the colour key indicate the distance in angstrom from the octahedral centre.

Figure 3. The structure of six-fold, P_6 , and four-fold, $P_4(1234)$, nanoparticle clusters as revealed by cryo-EM and 3D reconstruction.

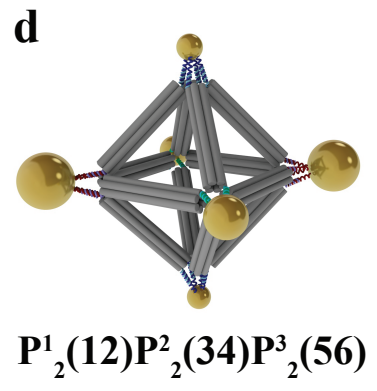
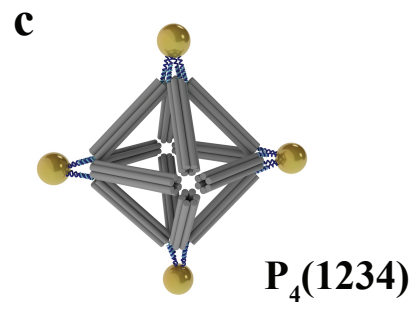
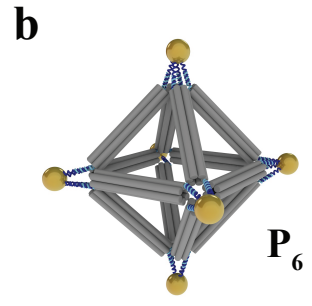
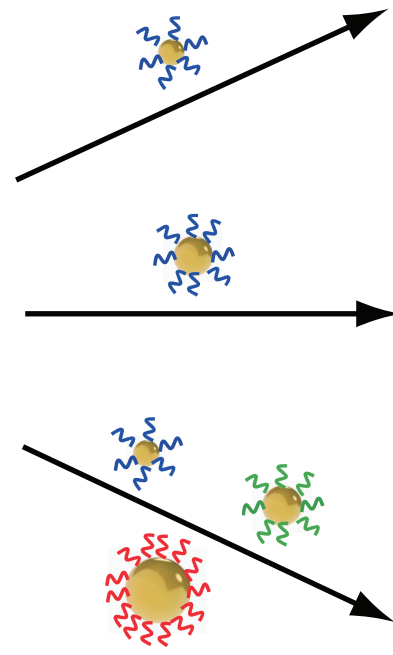
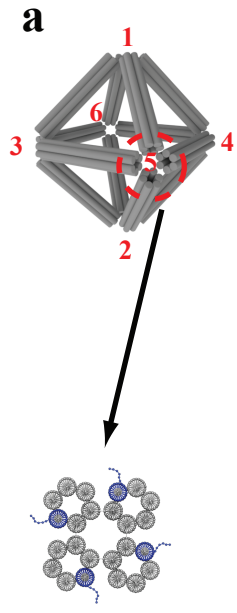
a, A representative EM image of the P_6 cluster structure. Inset shows the histogram of assembled clusters with observed nanoparticle numbers. **b**, Ten selected cryo-EM images of the fully assembled P_6 octahedron-nanoparticle clusters (second and fourth rows), in comparison with the 3D design model in corresponding views (first and third rows). **c**, The composite 3D EM structure of the P_6 cluster derived by computationally combining the structures shown in Supplementary Figure 5b and 5c. The left, middle, and right panel shows 4-fold, 3-fold, and 2-fold views of the respective structure. **d**, The cluster population histogram for $P_4(1234)$. **e**, Six selected raw cryo-EM images of the assembled $P_4(1234)$ cluster (bottom row) in comparison with the design model in corresponding views (top row). **f**, A composite density map of $P_4(1234)$ cluster derived by combining 3D reconstruction of the DNA octahedron (Figure 2c) with 3D reconstruction of the four 10-nm nanoparticles organized by octahedral DNA frame. The rendering threshold of the later is set to show

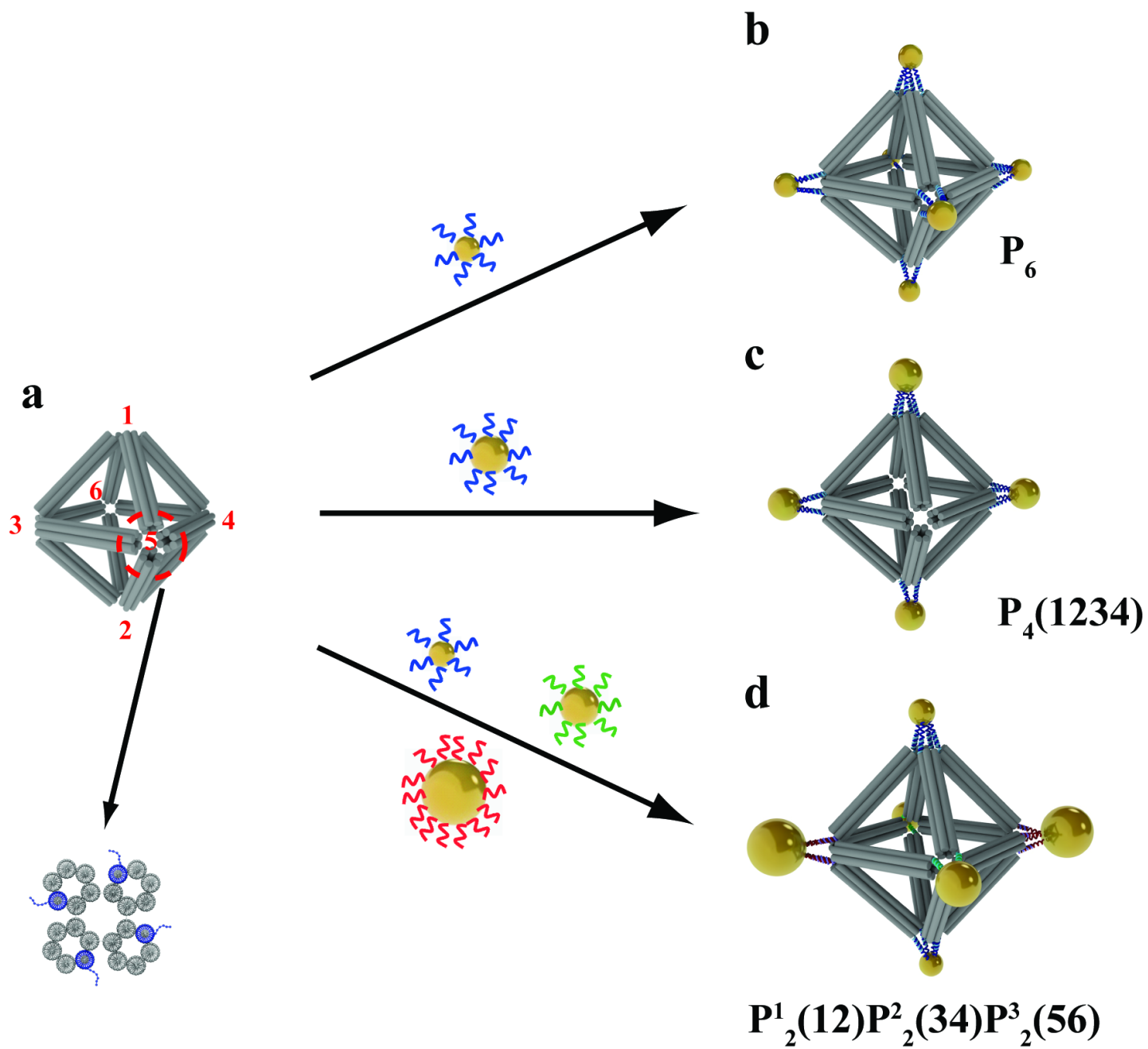
the nanoparticle densities. Left, middle, and right panel show view along the four-fold, three-fold, and two-fold symmetry axis of octahedron. Density surfaces of DNA octahedron in panel **c** and **f** are coloured in the same way as that in Figure 2c.

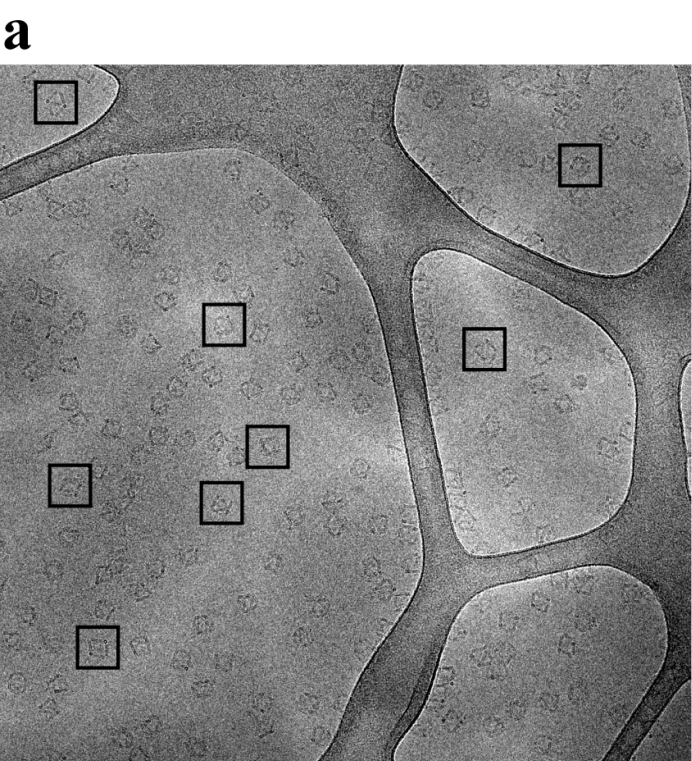
Figure 4. The characterization of hetero-cluster population and the structure of individual hetero-clusters, $P^1_2(12)P^2_2(34)P^3_2(56)$. **a**, Statistical analysis of the nanoparticle cluster population. The design model and a representative cryo-EM image of the assembled cluster (untilted view) are shown as insets. **b**, Reconstructed 3D structure of the nanoparticle cluster shown on the inset of (a). The surface-to-surface distance between the diagonally paired 7-nm, 10-nm, and 15-nm nanoparticles are denoted by d_7 , d_{10} , and d_{15} , respectively. α is the angle centred around the 10-nm nanoparticles, and β around the 15-nm nanoparticles, respectively. **c**, Images obtained by tilting the cluster shown in (a) at different angles (from left to right: -20° , -10° , 20° , 40° , 60°) (top row), in comparison with corresponding views of the reconstructed 3D structure. **d**, Averaged distances between the diagonally paired 7-, 10-, and 15-nm nanoparticles measured from 12 independently reconstructed $P^1_2P^2_2P^3_2$ clusters: $d_{15} = 58.0 \pm 4.8$ nm, $d_{10} = 55.1 \pm 5.6$ nm, and $d_7 = 53.3 \pm 5.3$ nm. **e**, Averaged values of the basal ($\alpha = 89.4^\circ \pm 10.9^\circ$) and vertex ($\beta = 54.5^\circ \pm 10.0^\circ$) angles.

Figure 5. CD spectra for non-chiral and chiral nanoparticle clusters assembled on octahedron frame. **a**, Model of non-chiral cluster $P^2_2P^3_2P^4_2$ with its top view. **b**, Model of chiral cluster $P^2_{c2}P^3_{c2}P^4_{c2}$ with its top view. **c**, Red line is the CD spectrum for cluster $P^2_2P^3_2P^4_2$. The representative TEM image and the model with same orientation are shown at the right top corner. Black line is the CD spectrum for cluster $P^2_{c2}P^3_{c2}P^4_{c2}$ and the blue line is the Lorentzian fit. The representative TEM image and model with same orientation are shown at the low left corner. The CD peaks at about 270 nm for both types of clusters are DNA signatures.

Figure 6. Correspondingly encoded octahedra used as programmable linkers for assembly into linear and 2D square arrays, respectively. **a**, Model of octahedral DNA origami with 2-fold symmetry nanoparticle binding for assembly of 1D array. **b**, The model of 1D array (upper) and the representative negative stained TEM image of formed 1D array (below). **c**, Extracted structure factor $S(q)$ for 1D array from in-situ SAXS pattern (red points is a measurement, and the blue line is fitting as described in the text). **d**, The model of octahedral DNA origami with 4-fold symmetry nanoparticle binding for assembly of 2D square array. **e**, The model of 2D square array and the representative negative stained TEM image of formed 2D nanoparticle-octahedra array (inset is a zoomed picture of selected area; bar scale is 25nm). **f**, Extracted structure factor $S(q)$ for 2D nanoparticle array (red line) and the simulated 2D scattering pattern (black lines with corresponding diffraction peak indexes).

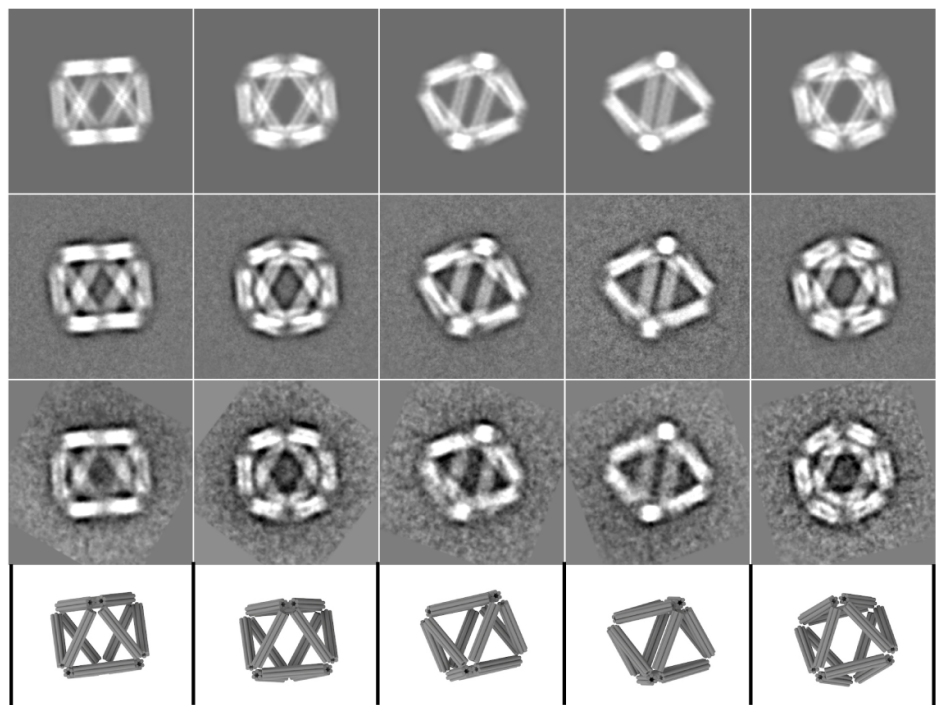






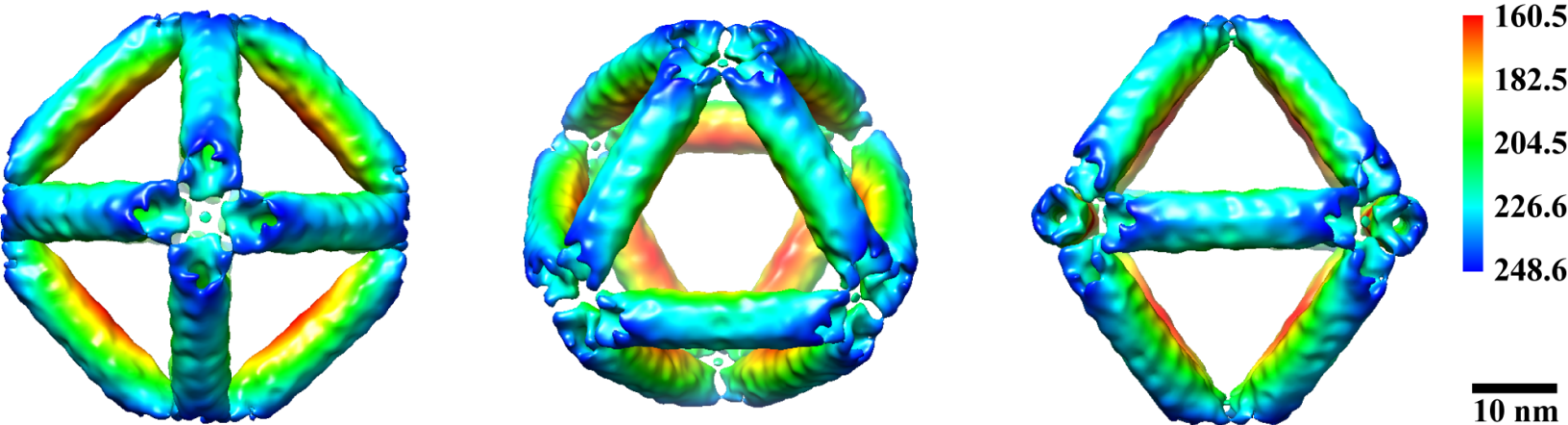
150 nm

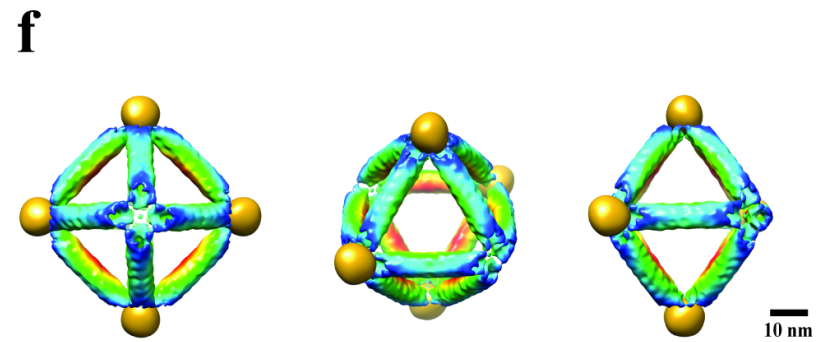
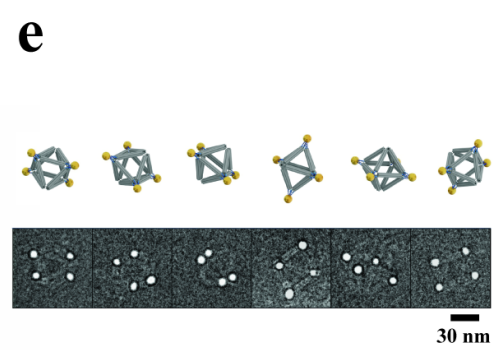
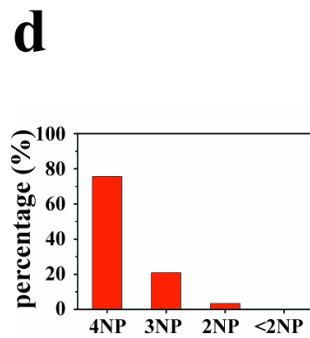
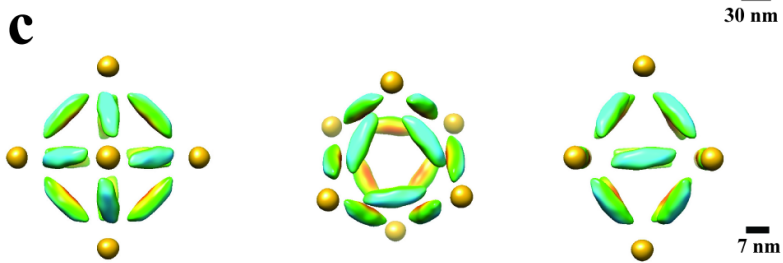
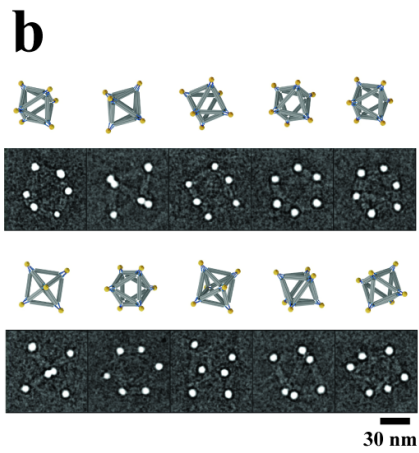
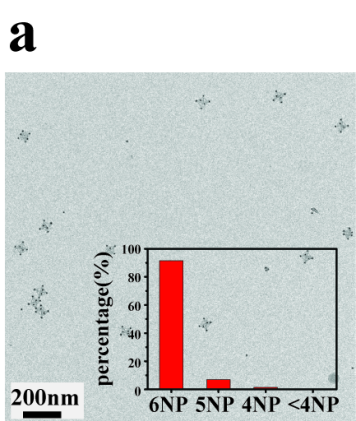
b

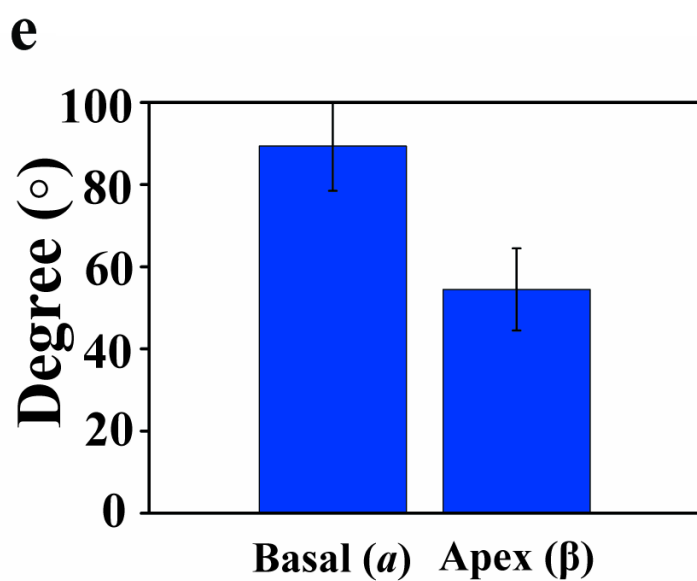
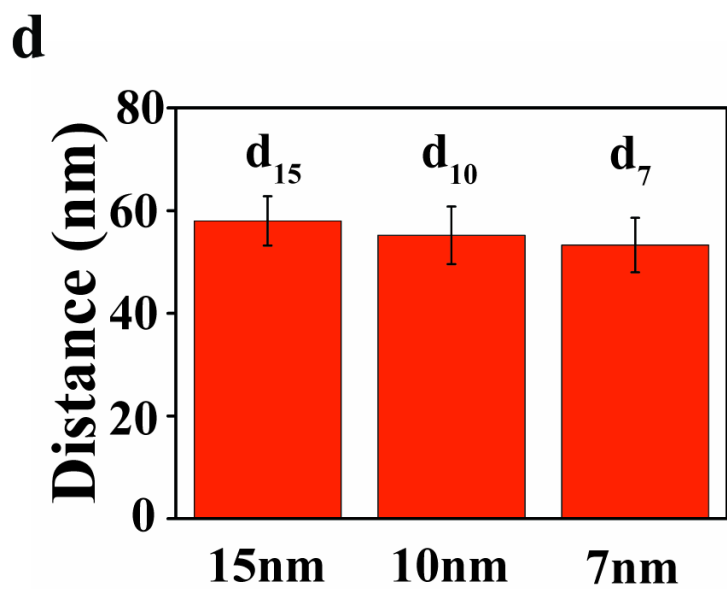
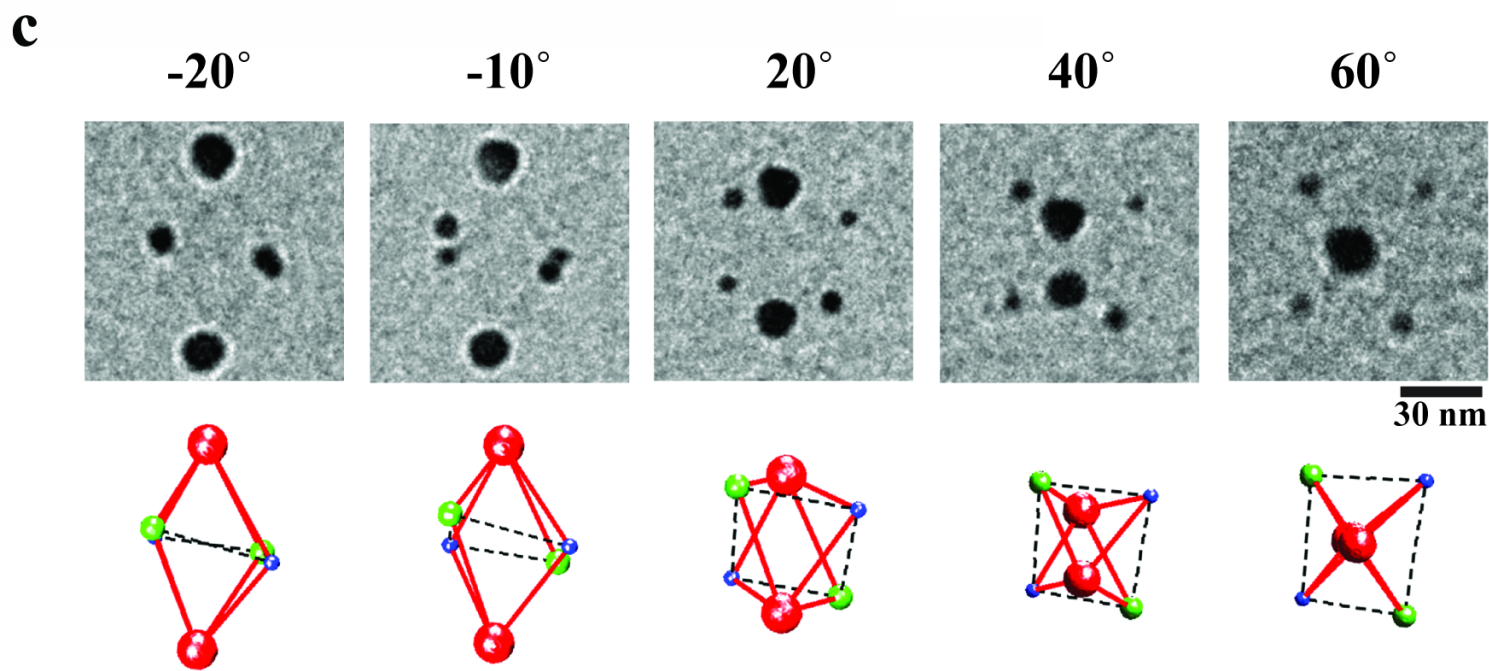
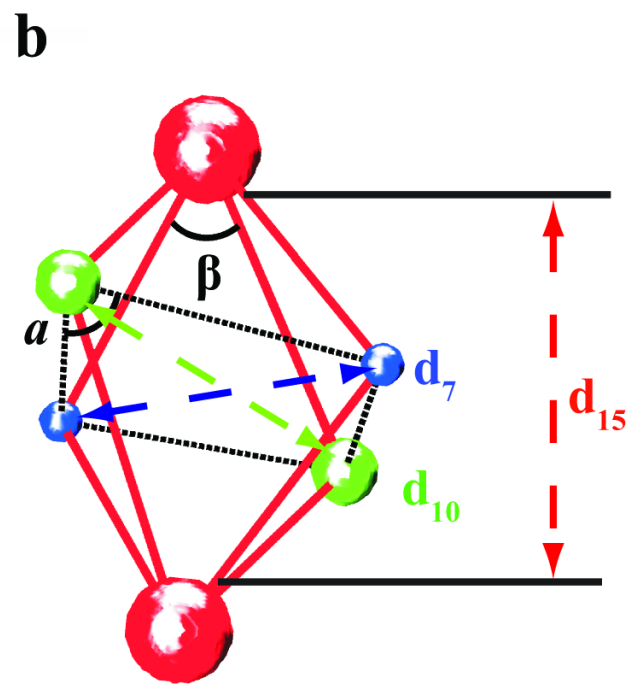
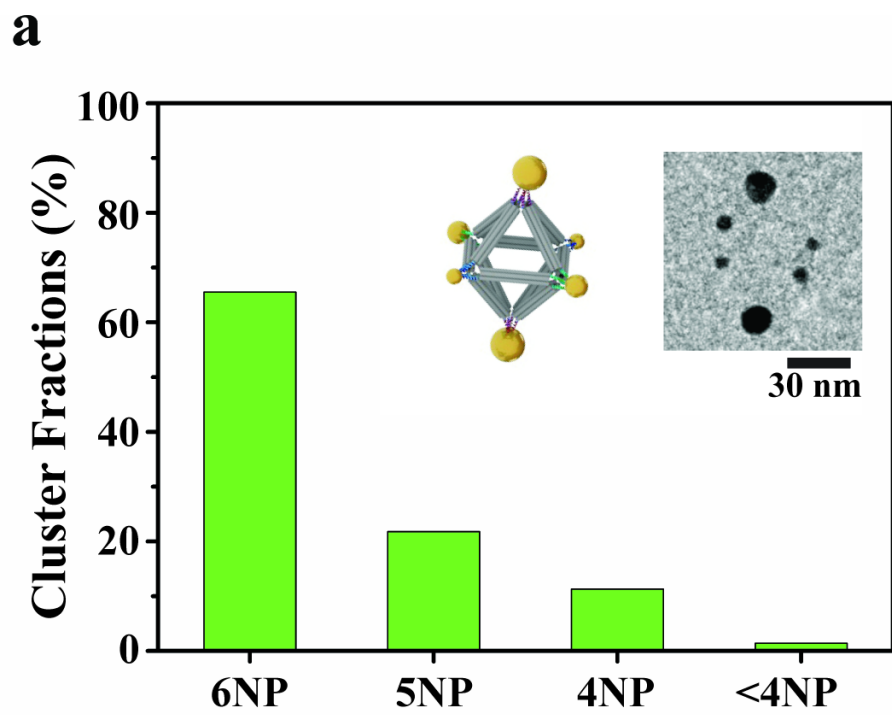


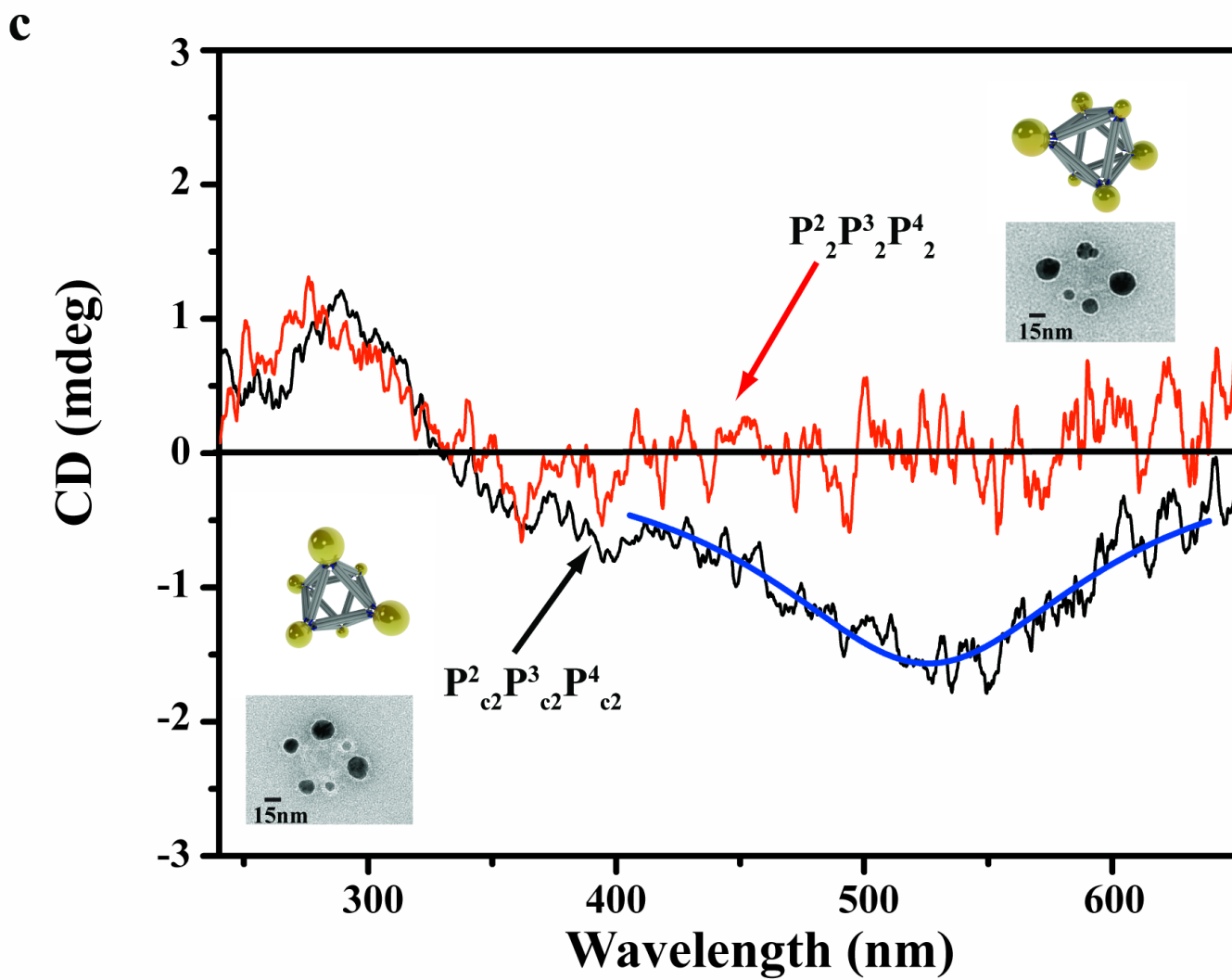
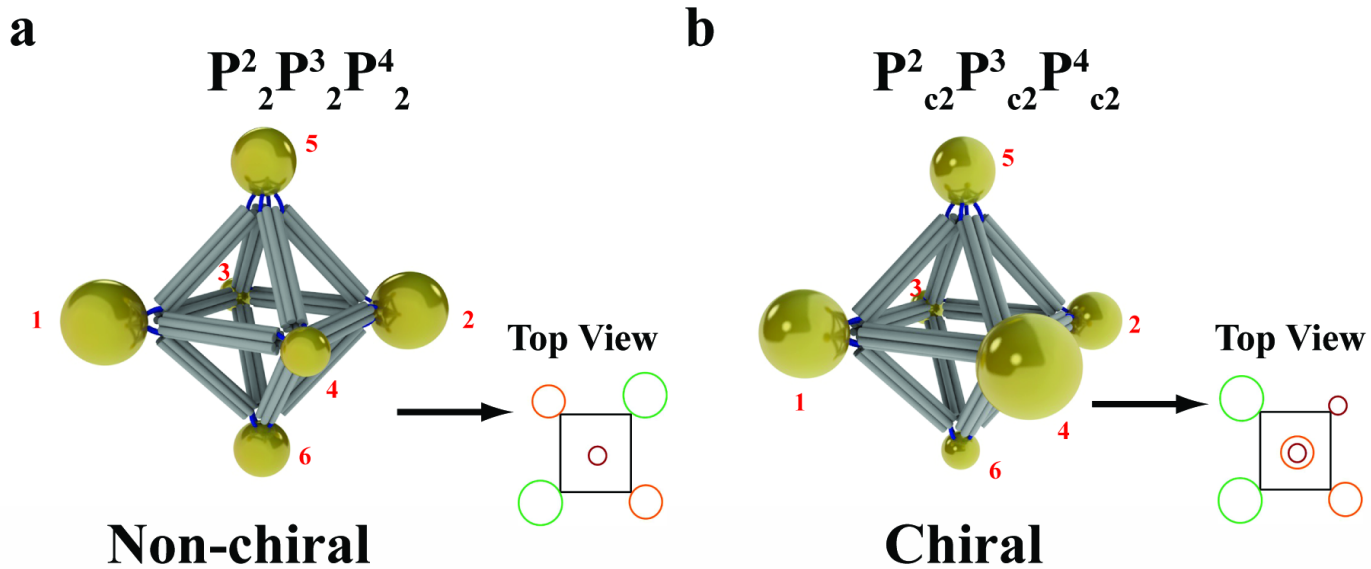
30 nm

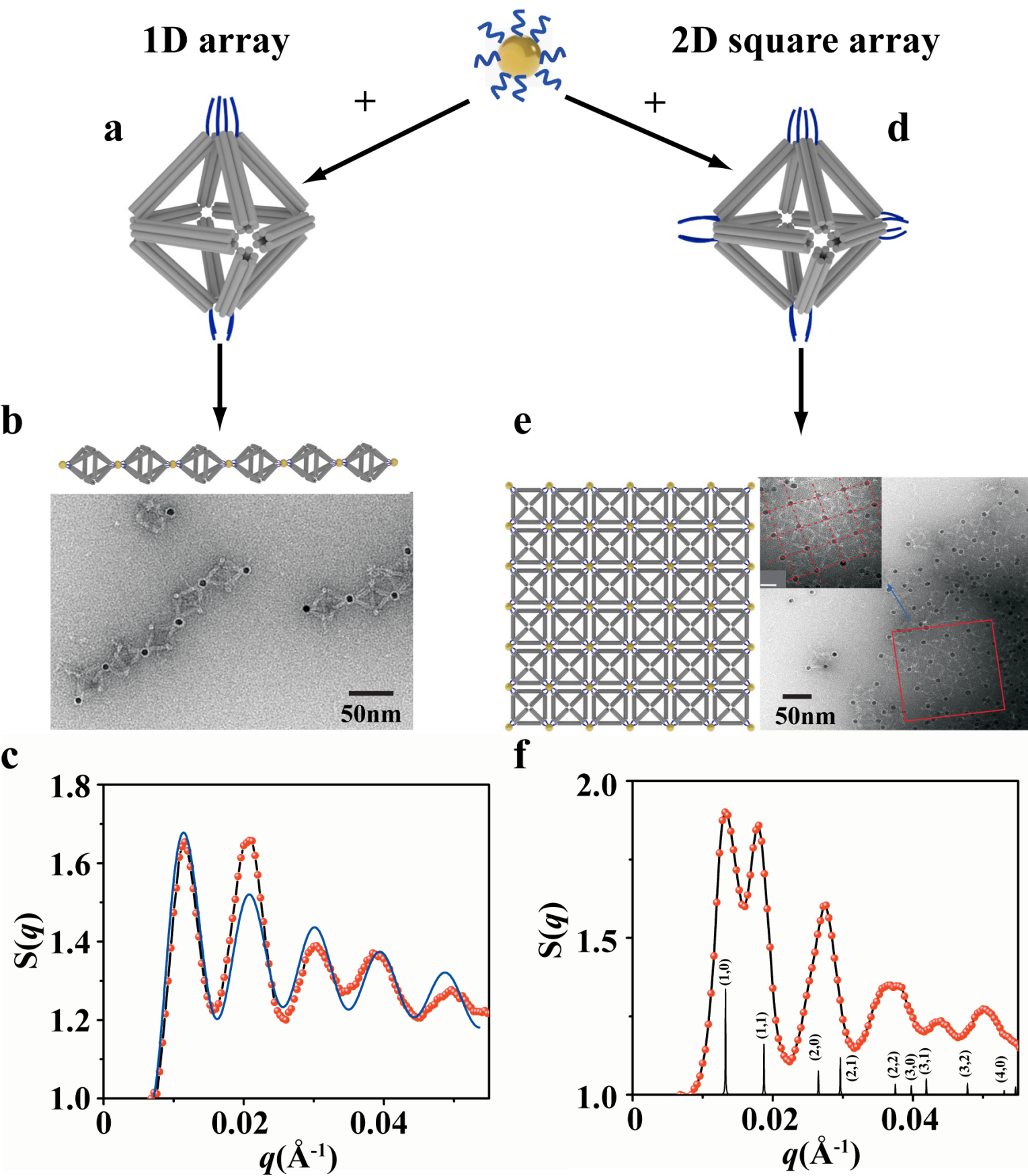
c











Methods

Design and folding of DNA octahedral frame. The DNA origami structure was designed using the caDNAno software package (<http://cadnano.org/>). Each edge of the octahedron was composed of a six-helix bundle with around 28.6nm, out of which one helix has a single strand DNA stretched out of the duplex ends for attaching nanoparticles. The octahedral DNA frame was formed by mixing M13mp18 DNA and hundreds of staple strands and slowly annealed from 90 °C to room temperature which was confirmed firstly by gel electrophoresis (Supplementary Figure 1).

Model fit of reconstructed octahedron. We computationally built a standard B-DNA model with 84 base pairs in length and manually arranged six copies to form a close-packed 6HB DNA model, leaving a hollow channel in the middle (see Supplementary information). We then docked the 6HB model as one entity (rigid body) into one edge of the DNA octahedron EM map, and found that the model fitted the density very well (Supplementary Figure 3). The good agreement leads us to conclude that we have succeeded in fabricating the DNA origami octahedron that we have designed for. The central cavity of the octahedron should be able to accommodate a spherical particle up to 20 nm in diameter.

Preparation of octahedral frame based nanoclusters. For assembly of each type of clusters shown in Figure 1b-1d, we first mixed gold nanoparticles with each designed frame by a ratio of 2.5N:1 (N means corner numbers which had sticky ends). The mixture was annealed from 50°C to room temperature overnight, concentrated, and loaded into agarose gel (1%) for separation. The gel band containing assembled clusters are cut out, crushed with a pestle, and filtered through a cellulose-acetate spin column, and the collected sample solution was used for negative-staining EM and cryo-EM.

Assembly of low-dimensional arrays. We mixed each design of octahedron with 10nm gold nanoparticles at the ratio of 1:1. After careful annealing (0.3 °C /h from 50 °C to 20 °C), red loose precipitates or black aggregates appeared gradually for 1D and 2D cases, respectively.

Small Angle X-ray Scattering (SAXS) profiles. SAXS measurements were performed at the BNL National Synchrotron Light Source (NSLS) X-9 beamline. The samples were injected into glass capillary tubes for x-ray scattering experiments that were performed under the temperature-controlled conditions. Two-dimensional scattering patterns were collected using the area detector. The structure factors, $S(q)$, where q is the wave vector, were obtained by the radial integration of two-dimensional patterns and were normalized by a nanoparticle form factor, obtained from the scattering of solution dispersed nanoparticles.